Chinese Chemical Letters 35 (2024) 108551

Contents lists available at ScienceDirect

Chinese Chemical Letters

journal homepage: www.elsevier.com/locate/cclet

Enhanced visible-light photocatalytic hydrogen evolution using two-dimensional carbon nitride sheets with the removal of amine groups

Yu Zhang[a,1,*], Liting Wu[b,1], Shaopeng Wang[b], Dingyi Yang[b], Huan Liang[b], Yizhang Wu[d,*], Jian Hao[e], Youqing Wang[a], Jianke Liu[a], Yong Wang[b,c,*]

[a] Department of Physics, Shaanxi University of Science and Technology, Xi'an 710021, China
[b] School of Advanced Materials and Nanotechnology, Academy of Advanced Interdisciplinary Research, Xidian University, Xi'an 710126, China
[c] The State Key Discipline Laboratory of Wide Band Gap Semiconductor Technology, Xidian University, Xi'an 710126, China
[d] Collaborative Innovation Center of Advanced Microstructures, National Laboratory of Solid State Microstructures, Nanjing University, Nanjing 210093, China
[e] State Key Laboratory of High-Efficiency Utilization of Coal and Green Chemical Engineering, Ningxia University, Yinchuan 750021, China

ARTICLE INFO

Article history:
Received 9 January 2023
Revised 9 April 2023
Accepted 9 May 2023
Available online 11 May 2023

Keywords:
2D carbon nitride sheets
Rapid thermal annealing
DFT calculations
Visible-light absorption
visible-light photocatalysis

ABSTRACT

Two-dimensional (2D) carbon nitride sheets (CNs) with atomically thin structures are regarded as one of the most promising materials for solar energy conversion. However, due to their substantially enlarged bandgap caused by the strong quantum size effect and their incomplete polymerisation with a large number of non-condensed surface amino groups, the practical applicability of CNs in photocatalysis is limited. In this study, CNs with broad visible-light absorption were synthesised using a 5-min fast thermal annealing. The removal of uncondensed amine groups reduces the bandgap of CNs from 3.06 eV to 2.60 eV, increasing their absorption of visible light. Interestingly, the CNs were distorted after annealing, which can differentiate the spatial positions of electrons and holes, enhancing the visible-light absorption efficiency. As a result, when exposed to visible light, the photocatalytic hydrogen production activity of atomically thin 2D CNs rose by 8.38 times. This research presents a dependable and speedy method for creating highly effective visible-light photocatalysts with narrowed bandgaps and improved visible-light absorption.

Hydrogen (H_2) generation *via* photocatalytic water splitting is a promising sustainable energy production method for addressing energy shortages and escalating environmental concerns [1–4]. To realize the practical benefits of this technology, reliable, high-efficiency and low-cost semiconductor photocatalysts must be developed [5–7]. Carbon nitride (CN) has sparked substantial interest as a metal-free semiconductor photocatalyst during the last decade due to its easy availability, low cost, excellent physicochemical stability and appealing electronic structure [8–11]. Unfortunately, due to the highly stacked layers, the bulk CN has a small surface area and quick electron-hole pair recombination, resulting in low photocatalytic activity [12,13]. Delaminating the bulk CN into atomically thin two-dimensional (2D) CN nanosheets (CNs) is a promising strategy for improving photocatalytic activity. CNs exhibit more exposed active sites, a larger specific surface area, shorter charge diffusion distances and improved photo-electronic properties as compared to bulk CNs [14–18]. However, due to the significantly increased bandgap caused by the strong quantum size effect, the use of atomically thin 2D CNs in photocatalysis is still unsatisfied [18,19]. More importantly, its incomplete polymerization with a large number of non-condensed surface amino groups results in an abundance of hydrogen bonding in the material layer [20,21]. These hydrogen bonds link the chains of polymer melon units. However, due to the weak interlayer force of hydrogen bonds, charge transfer between melon chains is difficult, resulting in poor interlayer transport [21–23]. As a result, CNs have a poor ability to transfer charge carriers and a limited capacity for photocatalysis.

To overcome these challenges, a range of techniques have been proposed, including coupling with aromatic compounds, heteroatom doping and fabrication defects [21,24–27]. To some extent, these approaches can boost CN absorbance and broaden its restricted visible-light absorption spectrum, hence improving photocatalytic efficacy. However, its complex procedures impeded its

* Corresponding authors.
E-mail addresses: zhangy0827@sust.edu.cn (Y. Zhang), yzwu@smail.nju.edu.cn (Y. Wu), yongwang@xidian.edu.cn (Y. Wang).
[1] These authors contributed equally to this work.

https://doi.org/10.1016/j.cclet.2023.108551
1001-8417/

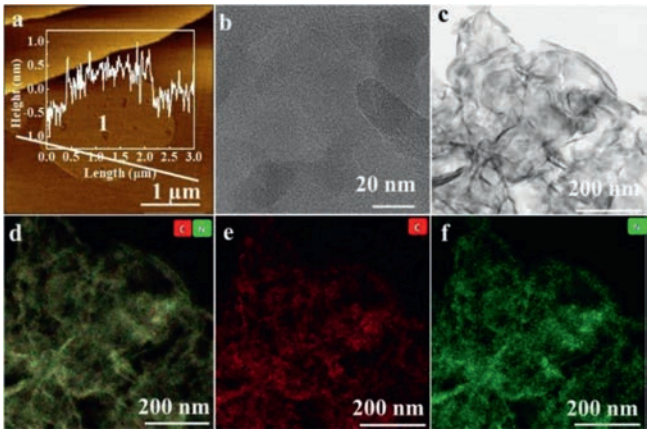

Fig. 1. AFM image and its cross-section height profile along the white line (a), TEM image (b), energy filtered STEM image (c) and EELS elemental mapping images of C and N (d–f) for CNs-640.

wider application. As a result, an efficient and facile strategy for extending CNs' visible-light absorption was required. A quick (5-min) annealing process was used to synthesise CNs with broad visible-light absorption. According to experimental and theoretical investigations, rapid heat annealing selectively breaks hydrogen bonds and uncondensed amine groups are removed to produce new N=CH–N bonds. By removing the amine group, the band gap of CNs can be reduced from 3.06 eV to 2.60 eV, increasing their absorption of visible light. Meanwhile, after annealing, the CNs were deformed, which can separate the spatial positions of electrons and holes, enhancing the visible-light absorption efficiency. As a result, when exposed to visible light, the photocatalytic hydrogen production activity of atomically thin 2D CNs was boosted by 8.38 times, reaching 6284.47 μmol g^{-1} h^{-1}.

An atomic force microscope (AFM) and transmission electron microscopy (TEM) were used to examine the surface morphology of the samples. We discovered that the CNs have a lateral dimension ranging from tens of nanometers to around one hundred nanometers (Fig. S1 in Supporting information), as previously described for atomically thin 2D CNs [18,28]. The thickness of CNs-640 after 5 min of thermal annealing was approximately 1 nm, as shown in Fig. 1a. Additionally, the TEM result in Fig. 1b shows similar morphology to that of CNs. Furthermore, the electron energy loss spectrum (EELS) in Figs. 1c–f confirmed the presence and consistent distribution of carbon and nitrogen elements in CNs-640.

The crystal structure of CNs was analysed using X-ray powder diffraction (XRD) patterns at different annealing temperatures for 5 min, as shown in Fig. 2a and Fig. S2 (Supporting information). The strength of the characteristic peaks at 13° (100) and 27.6° (002) progressively decreased with increasing annealing temperature, implying that the interlayer hydrogen bonds were gradually broken [29,30]. The peaks almost completely vanished when the temperature reached 680 °C, indicating that the hydrogen bonds were completely broken and the periodic structure of CNs was destroyed. The yield of CNs gradually decreases at each temperature also further verified the structure of CNs was destroyed (Table S1 in Supporting information). The peak at 476.2 cm^{-1} was observed in the Raman spectrum, which is the characteristic peak of CNs (Fig. S3 in Supporting information) [16,21]. The Fourier transform infrared (FTIR) spectra of the samples showed that the feature bands were enhanced at 810 cm^{-1} and decreased between 3100 cm^{-1} and 3300 cm^{-1} compared to CNs, as shown in Fig. 2b and Fig. S4 (Supporting information).

It can be concluded that selective hydrogen bond destruction affects the periodic arrangement of melon chains within layers and

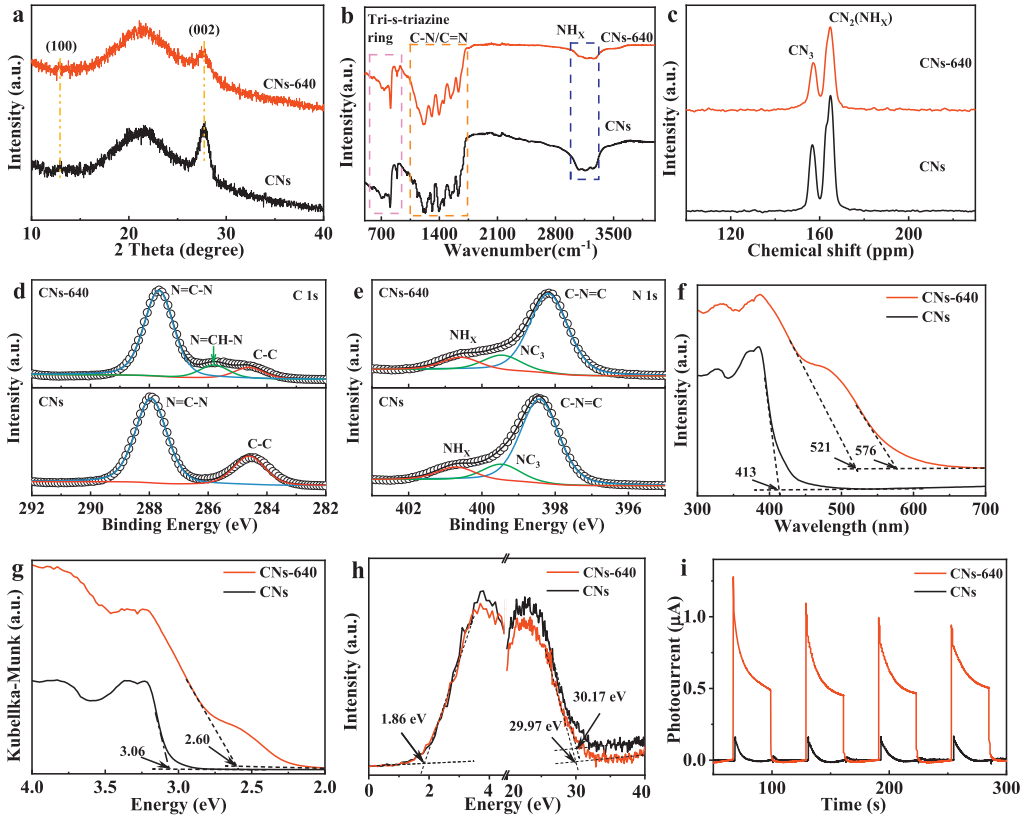

Fig. 2. XRD patterns (a), FTIR spectra (b), solid NMR spectra of ^{13}C (c), C 1s XPS spectra (d), N 1s XPS spectra (e), UV–vis absorption spectra (f), transformed Kubelka–Munk *vs.* light energy plots (g), UPS spectra (h) and transient photocurrent responses under visible light (i) for CNs and CNs-640.

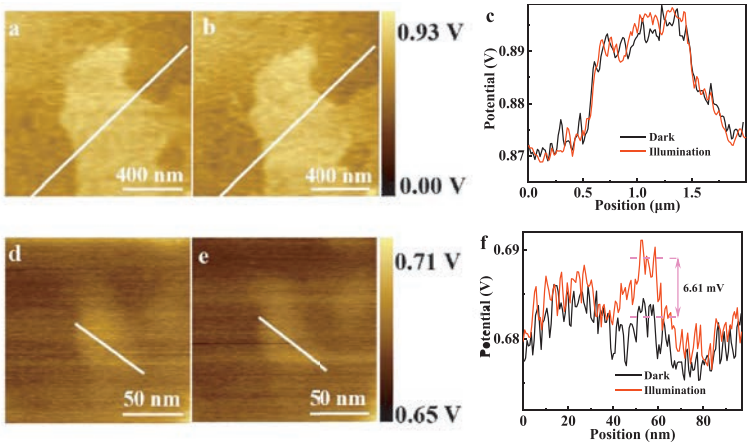

Fig. 3. SPV images of CNs under dark conditions (a), under illumination (b) and corresponding surface potential (c). SPV images of CNs under dark conditions (d), under illumination (e) and corresponding surface potential (f).

reduces the number of uncondensed amine groups. The atomic structure's framework is then preserved [29,31–33]. The sample with an annealing temperature of 680 °C has almost no characteristic bands, indicating that the structure has been destroyed, as indicated by the XRD results. The ^{13}C nuclear magnetic resonance (NMR) results in Fig. 2c show that after annealing at 640 °C, the ratio of the peak intensity of CN_3 to that of $CN_2(NH_X)$ increases from 0.57 to 0.81, ascribed to the loss of uncondensed amine groups [14,34]. Based on the results discussed above, it is clear that the hydrogen bonds were selectively destructed during annealing, and the uncondensed amine groups were lost.

X-ray photoelectron spectroscopy (XPS) measurements were used to further investigate the surface chemical properties of the as-prepared samples. As illustrated in Fig. 2d, two peaks in the C 1s spectrum were observed at 284.6 eV and 287.94 eV, which are attributed to C-C and N=C–N, respectively [35,36]. In addition, a CNs-640 peak at 285.8 eV emerged, corresponding to an N=CH–N bond [14,24]. The C–N=C (398.4 eV), NC_3 (399.5 eV) and NH_X (400.7 eV) bands are assigned to the N 1s spectrum (Fig. 2e) [37,38]. Meanwhile, the NH_X/N_2C peak area ratio of CNs decreased from 0.153 to 0.144, and the NH_X/NC_3 ratio decreased from 0.774 to 0.731 (Table S2 in Supporting information), indicating that the more uncondensed amino groups in CNs, the more amine groups were lost during annealing [14,39]. According to the experimental findings, the amine group can be removed from the melon strands during rapid thermal annealing by breaking hydrogen bonds, the long-range atomic order structure of the chain between layers was disrupted, and a new N=CH–N bond is formed.

We used UV–visible absorption spectroscopy (UV–vis) to determine the optical properties of samples. The absorption edge of CNs is 415 nm, as shown in Figs. 2f and g and Figs. S5 and S6, and the corresponding band gap is calculated as 3.06 eV from the Kubelka–Munk (K-M) curve. With increasing temperature and rapid thermal annealing, the absorption edge can be red-shifted to 576 nm, and the band gap can be narrowed to 2.60 eV. This suggests that removing the amine group can narrow the bandgap and significantly improve the use of solar light with a broader band. The narrowing of the bandgap can effectively promote the effective separation between photoexcited electrons and holes, which is crucial for improving photocatalytic performance [40,41]. Fig. 2h depicts the high and low kinetic energy regions of CNs and CNs-640, where the incident photon energy is 40.8 eV, and the conduction band minimum of CNs-640 is 0.66 eV higher than that of CNs (Table S3 in Supporting information) [42–44]. The enhancement of the conduction band minimum can provide the driving force for the photocatalytic reduction of hydrogen protons, ultimately improving

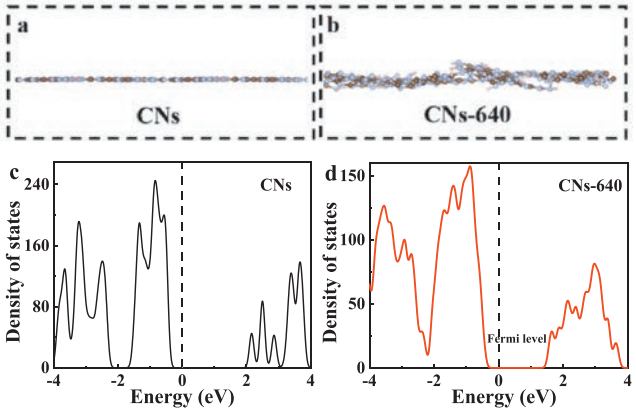

Fig. 4. Side views of the optimized structure of CNs (a) and CNs-640 (b). Density of states (DOS) of CNs (c) and CNs-640 (d).

the efficiency of H_2 production [45,46]. Furthermore, CNs-640 has a higher photocurrent density than CNs (Fig. 2i), suggesting that the rapid thermal annealing process improves charge transfer and separation, both of which are beneficial to photocatalytic activity.

To further explore the separation and recombination of photogenerated carriers in the samples after rapid thermal annealing, we performed surface photovoltage (SPV) measurements as shown in Fig. 3. We discovered from Figs. 3a–c that light had little effect on the intensity of CNs. The CNs-640 sample showed a differential surface potential change of 6.61 mV after rapid thermal annealing (Figs. 3d–f). As a result, rapid thermal annealing may be used to suppress photogenerated carrier recombination. According to the above experimental findings, quick thermal annealing can selectively break hydrogen bonds and form N=CH–N bonds, remove amine groups and narrow the band gap, increase visible-light absorption and facilitate photogenerated carrier separation.

To further understand the photocatalytic ability of the sample after rapid thermal annealing, the first-principles density functional theory (DFT) calculations were performed as shown in Fig. 4. We can see in Figs. 4a and b that the 2D planar CNs were distorted after 5 ps of simulated annealing at 913 K. By removing NH_3 molecules, the sample condenses, increasing the C/N ratio while decreasing the H content. As a result, interchain –NH– bonds are generated at 913 K, leading to the deformation of the triazine/heptazine unit, thereby deforming the 2D planar structure of CNs [47]. This structural distortion phenomenon disrupts local

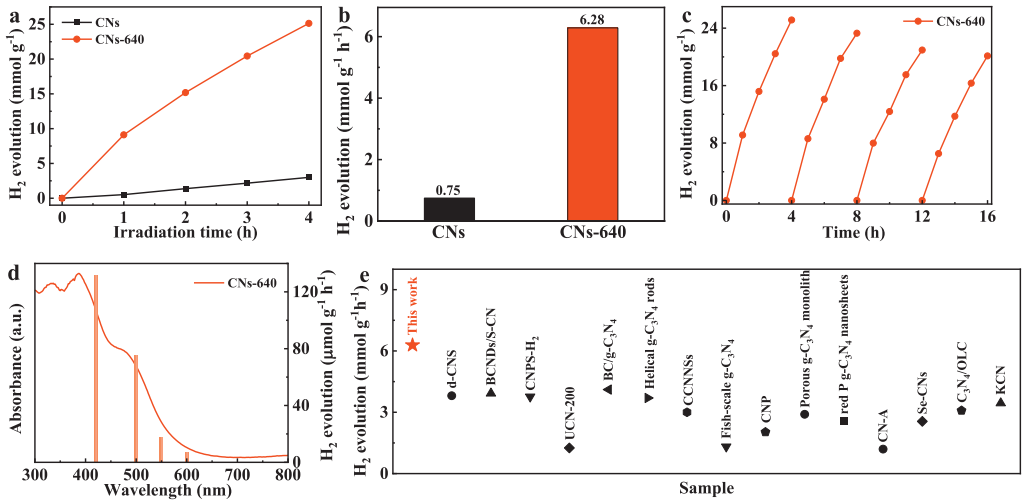

Fig. 5. Hydrogen evolution (a) and hydrogen evolution rate (b) for CNs and CNs-640. Stability of hydrogen evolution (c) and wavelength dependent photocatalytic hydrogen production rate (d) for CNs-640. Comparison of hydrogen evolution with CNs-640 over reported CN photocatalyst with Pt as cocatalyst (e) [14,50–63].

symmetry in the form of C and N atoms, separating electron and hole spatial positions and improving visible-light absorption efficiency [48,49]. The band gaps of CNs and CNs-640 are 2.23 and 1.67 eV, respectively, as shown in Figs. 4c and d. Clearly, rapid thermal annealing reduces the band gap of CNs-640. As a result, CNs-640 is expected to have more charge carriers, which will improve photoresponsivity. Based on the above experimental and computational results, we can conclude that removing amine groups after rapid thermal annealing can narrow the band gap of CNs and facilitate photogenerated carrier separation. Then, to improve hydrogen production efficiency, visible-light absorption can be increased.

We used 10 vol% TEOA as a sacrificial agent and 3 wt% Pt cocatalyst to examine the photocatalytic hydrogen generation activities of the samples under visible-light irradiation ($\lambda > 420$ nm). As illustrated in Fig. 5a and Fig. S7 (Supporting information). The yield of the samples increased gradually as the rapid thermal annealing temperature was raised. When the temperature reached 640 °C, CNs-640 produced 25,137.89 μmol/g) of H_2, which was 8.38 times that of CNs (only 2998.95 μmol/g). The yield of structurally altered CNs-680, on the other hand, was extremely low at 484.92 μmol/g. The corresponding hydrogen production rate, shown in Fig. 5b and Fig. S8 (Supporting information), where the CNs-640 was 6284.47 μmol g^{-1} h^{-1} (CNs was 749.74 μmol g^{-1} h^{-1}). Furthermore, CNs-640 demonstrated good photocatalytic stability, with no discernible drop in photocatalytic H_2 production over four cycles (Fig. 5c). As shown in Fig. 5d, the activity of CNs-640 is consistent with its optical absorption spectrum at different wavelengths, implying that photo-induced electrons in CNs-640 are primarily responsible for driving H_2 evolution. The H_2 production rates of typical photocatalysts reported so far are summarised in Fig. 5e and Table S4 (Supporting information), and the samples used in this paper produce more hydrogen. As a result, rapid thermal annealing of the samples increased visible-light absorption, promoted photogenerated carrier separation and improved the photocatalytic hydrogen evolution reaction.

In summary, rapid thermal annealing was used to successfully prepare highly efficient visible-light photocatalysts. When exposed to visible light, atomically thin 2D CNs exhibit photocatalytic hydrogen production activity of 6284.47 μmol g^{-1} h^{-1}, which is 8.38 times greater than that of CNs. Experiment results and theoretical studies show that hydrogen bonds can be selectively broken by rapid thermal annealing to form new N=CH–N bonds and uncondensed amine groups can be removed to reduce the bandgap of CNs from 3.06 eV to 2.60 eV, enhancing their visible-light absorption. After annealing, the CNs were distorted, which separates the spatial positions of electrons and holes, improving the visible-light absorption efficiency. This research provides a dependable and rapid method for developing highly efficient visible-light photocatalysts with narrowed bandgaps and enhanced visible-light absorption.

Declaration of competing interest

The authors declare that they have no known competing financial interests or personal relationships that could have appeared to influence the work reported in this paper.

Acknowledgments

This work was supported by the National Natural Science Foundation of China (Nos. 12104352 and 12204294), Fundamental Research Funds for the Central Universities (Nos. XJS212208 and 2020BJ-56), and Foundation of State Key Laboratory of High-efficiency Utilization of Coal and Green Chemical Engineering (No. 2022-K67), the Natural Science Foundation of Shaanxi Province (Nos. 2019JCW-17 and 2020JCW-15).

Supplementary materials

Supplementary material associated with this article can be found, in the online version, at doi:10.1016/j.cclet.2023.108551.

References

[1] S. Patnaik, S. Martha, S. Acharya, K.M. Parida, Inorg. Chem. Front. 3 (2016) 336–347.
[2] N. Kanjana, W. Maiaugree, P. Poolcharuansin, P. Laokul, J. Mater. Sci. Technol. 48 (2020) 105–113.
[3] Y. Wu, W. Xiong, Z. Wang, et al., Chem. Eng. J. 427 (2022) 131925.
[4] J. Liu, S. Zhu, B. Wang, et al., Chin. Chem. Lett. 34 (2023) 107749.
[5] Y. Wang, M. Sun, W. Tang, et al., Mater. Today Phys. 23 (2022) 100634.
[6] J. Nie, G. Zhu, W. Zhang, et al., Chem. Eng. J. 424 (2021) 130327.
[7] Q. Li, C. Ren, C. Qiu, et al., Chin. Chem. Lett. 32 (2021) 3463–3468.
[8] X. Zhang, F. Tian, X. Lan, et al., Chem. Eng. J. 429 (2022) 132588.
[9] Y. Orooji, M. Ghanbari, O. Amiri, M. Salavati-Niasari, J. Hazard. Mater. 389 (2020) 122079.
[10] Y. Wang, C. Zeng, L. Wu, et al., J. Mater. Sci. Technol. 146 (2023) 113–120.
[11] Z. Chen, B. Chong, N. Wells, et al., Chin. Chem. Lett. 33 (2022) 2579–2584.
[12] Z. Zhao, Z. Shu, J. Zhou, et al., Mater. Res. Bull. 145 (2022) 111565.
[13] C. He, W. Xia, C. Zhou, et al., Chem. Eng. J. 430 (2022) 132751.
[14] Y. Wang, P. Du, H. Pan, et al., Adv. Mater. 31 (2019) e1807540.
[15] T. Su, Q. Shao, Z. Qin, et al., ACS Catal. 8 (2018) 2253–2276.
[16] Y. Wang, W. Xu, Y. Zhang, et al., Energy Environ. Mater. 0 (2022) 1–9.

[17] M. Aggarwal, S. Basu, N.P. Shetti, et al., Chem. Eng. J. 425 (2021) 131402.
[18] Y. Wang, Y. Guo, C. Zeng, et al., Nano Energy 104 (2022) 107983.
[19] Y. Wang, C. Zeng, Y. Zhang, et al., Mater. Today Phys. 22 (2022) 100600.
[20] A. Thomas, A. Fischer, F. Goettmann, et al., J. Mater. Chem. 18 (2008) 4893.
[21] Y. Wang, Y. Zhang, Y. Wang, et al., ACS Appl. Mater. Interfaces 13 (2021) 40629–40637.
[22] L. Lin, Z. Yu, X. Wang, Angew. Chem. Int. Ed. 58 (2019) 6164–6175.
[23] S.F. Ng, J.J. Foo, W.J. Ong, InfoMat 4 (2022) e12279.
[24] Y. Zhang, Y. Wang, W. Xu, et al., Chem. Eng. J. 431 (2022) 133219.
[25] S. Li, Z. Niu, D. Pan, et al., Chin. Chem. Lett. 33 (2022) 3581–3584.
[26] Y. Xing, X. Wang, S. Hao, et al., Chin. Chem. Lett. 32 (2021) 13–20.
[27] C. Zhou, Y. Liang, W. Xia, et al., J. Hazard. Mater. 441 (2023) 129871.
[28] Y. Yang, L. Geng, Y. Guo, et al., Appl. Surf. Sci. 425 (2017) 535–546.
[29] Y. Kang, Y. Yang, L.C. Yin, et al., Adv. Mater. 28 (2016) 6471–6477.
[30] F. Fina, S.K. Callear, G.M. Carins, J.T.S. Irvine, Chem. Mater. 27 (2015) 2612–2618.
[31] H. Yu, R. Shi, Y. Zhao, et al., Adv. Mater. 29 (2017) 1605148.
[32] Y. Kang, Y. Yang, L.C. Yin, et al., Adv. Mater. 27 (2015) 4572–4577.
[33] B.V. Lotsch, M. Doblinger, J. Sehnert, et al., Chemistry 13 (2007) 4969–4980 (Easton).
[34] Y. Wang, W. Xu, Y. Zhang, et al., Nano Energy 83 (2021) 105783.
[35] Z. Tong, D. Yang, Z. Li, et al., ACS Nano 11 (2017) 1103–1112.
[36] Q. Liang, Z. Li, Z.-H. Huang, et al., Adv. Funct. Mater. 25 (2015) 6885–6892.
[37] W. Li, Y. Wang, X. Yang, et al., ACS Appl. Nano Mater. 2 (2019) 7559–7565.
[38] K. Xiao, P. Giusto, L. Wen, et al., Angew. Chem. Int. Ed. 57 (2018) 10123–10126.
[39] X. Song, D. Tang, Y. Chen, et al., ACS Omega 4 (2019) 6114–6125.
[40] C. Zhou, E. Almatrafi, X. Tang, et al., Sep. Purif. Technol. 286 (2022) 120464.
[41] X. Chen, S. Shen, L. Guo, S.S. Mao, Chem. Rev. 110 (2010) 6503–6570.
[42] X. Tao, Y. Gao, S. Wang, et al., Adv. Energy Mater. 9 (2019) 1803951.
[43] D. Kim, K. Yong, Appl. Catal. B 282 (2021) 119538.
[44] M. Li, X. Tu, Y. Wang, et al., Nanomicro. Lett. 10 (2018) 45.
[45] H. Zhang, J. Lin, Z. Li, et al., Catal. Sci. Technol. 9 (2019) 502–508.
[46] Q. Han, B. Wang, J. Gao, et al., ACS Nano 10 (2016) 2745–2751.
[47] A.B. Jorge, D.J. Martin, M.T.S. Dhanoa, et al., J. Phys. Chem. C 117 (2013) 7178–7185.
[48] Y. Chen, B. Wang, S. Lin, et al., J. Phys. Chem. C 118 (2014) 29981–29989.
[49] H. Kim, S. Gim, T.H. Jeon, et al., ACS Appl. Mater. Interfaces 9 (2017) 40360–40368.
[50] M. Liu, Y. Jiao, J. Qin, et al., Appl. Surf. Sci. 541 (2021) 148558.
[51] N. Meng, J. Ren, Y. Liu, et al., Energ. Environ. Sci. 11 (2018) 566–571.
[52] L. Chen, X. Liang, H. Wang, et al., Chem. Eng. J. 442 (2022) 136115.
[53] Y. Lu, W. Wang, H. Cheng, et al., Int. J. Hydrog. Energy 47 (2022) 3733–3740.
[54] Y. Zheng, L. Lin, X. Ye, et al., Angew. Chem. Int. Ed. 53 (2014) 11926–11930.
[55] H. Ou, L. Lin, Y. Zheng, et al., Adv. Mater. 29 (2017) 1700008.
[56] B. Lin, H. An, X. Yan, et al., Appl. Catal. B 210 (2017) 173–183.
[57] C. Wang, W. Wang, H. Fan, et al., ACS Appl. Mater. Interfaces 12 (2020) 5234–5243.
[58] Q. Liang, Z. Li, X. Yu, et al., Adv. Mater. 27 (2015) 4634–4639.
[59] L. Jing, R. Zhu, D.L. Phillips, J.C. Yu, Adv. Funct. Mater. 27 (2017) 1703484.
[60] N. Sun, X. Wen, Y. Tan, et al., Appl. Surf. Sci. 470 (2019) 724–732.
[61] Y. Zhang, Y. Wang, M. Di, et al., Chem. Eng. J. 385 (2020) 123938.
[62] Y. Shi, Q. Zhao, J. Li, et al., Appl. Catal. B 308 (2022) 121216.
[63] H. Jing, L. Chen, S. Yi, et al., Chem. Eng. J. 417 (2021) 129187.